MULTI-RADIATION MODELLING OF THE PLASMA FOCUS

S Lee[1,2,3*] and S H Saw[1,2]

[1]INTI International University, 71800 Nilai, Malaysia
[2]Institute for Plasma Focus Studies, Melbourne, Australia
[3]National Institute of Education, Nanyang Technological University, Singapore

e-mails: sorheoh.saw@newinti.edu.my leesing@optusnet.com.au

*Corresponding author: Prof Dr S Lee
Mailing Address: Institute for Plasma Focus Studies
32 Oakpark Drive
Chadstone VIC3148
Australia

Tel No: +61 (0)451576282

Short Title: Multi-Radiation Modelling of the Plasma Focus

Number of:
Pages: 17
Tables: 0
Figures: 8

MULTI-RADIATION MODELLING OF THE PLASMA FOCUS

S Lee[1,2,3*] and S H Saw[1,2]

[1]INTI International University, Nilai, Malaysia
[2]Institute for Plasma Focus Studies, Melbourne, Australia
[3]National Institute of Education, Nanyang Technological University, Singapore

The Plasma Focus has wide-ranging application potential due to its intense radiation of SXR, XR, electron and ion beams and fusion neutrons when operated in Deuterium. We discuss here the 5-phase Lee Model code for the focus operated in various gases generally and using examples drawn from D, D-T, He, Ne, N, O, Ar, Kr and Xe. For D, D-T and He a fully ionized model is used. For the heavier gases from Ne onwards a corona model is used to generate the thermodynamic data required in the computation. The use of gases such as Ne and Xe for generation of specific SXR or EUV lines for micro-lithography applications has been discussed in the literature as has use of N and O to generate lines suitable for water-window microscopy. Recently Ar was considered for micro-machining due to the harder characteristic line radiation. Various doping gases including Kr have been used for fusion neutron yield enhancement due arguably to mechanisms such as thermodynamically enhanced pinch compressions. In this paper we also look at the effect of radiation cooling and radiation collapse in the heavier noble gases. The Pease-Braginskii current is known to be that current flowing in a hydrogen pinch which is just large enough for the Bremsstrahlung to balance Joule heating. This radiation-cooled threshold current for a hydrogen pinch is 1.6MA. It is known that in gases undergoing line radiation strongly the radiation-cooled threshold current is considerably lowered. We show that the equations of the Lee Model code may be used to compute this lowering. The code also shows the effect of radiation cooling when operated in the relevant regimes. It is suggested that the neutron enhancement effect of seeding could at least in part be due to the enhanced compression caused by radiation cooling probably in localized regions.

Keywords: Plasma Focus numerical experiments, Plasma Focus Scaling, Radiation Cooling, Radiation Collapse, Plasma Focus Radiation Enhancement

1. Introduction

The Plasma Focus has wide-ranging application potential due to its intense radiation of SXR, XR, electron and ion beams and fusion neutrons [1] when operated in Deuterium. The use of gases such as Ne and Xe for generation of specific SXR or EUV lines for micro-lithography applications [2,3,4] has been widely discussed in the literature as has the use of N and O to generate the lines suitable for water-window microscopy [5]. Recently Ar has been considered for micro-machining due to the harder characteristic line radiation [6]. Various gases including Kr have been discussed and used for fusion neutron yield enhancement due arguably to mechanisms such as thermodynamically enhanced pinch compressions. In this paper we also look at the effect of radiation cooling and radiation collapse in the heavier noble gases. The Pease-Braginskii current [7] is known to be that current flowing in a hydrogen pinch which is just large enough for the Bremsstrahlung to balance Joule heating. This radiation-cooled threshold current for a hydrogen pinch is 1.6MA. It is known that in gases undergoing line radiation strongly the radiation-cooled threshold current is considerably lowered. We show that the equations of the Lee Model code [8] may be used to compute this lowering. The code also shows the effect of radiation cooling when operated in the relevant regimes. It is suggested that the neutron enhancement effect of seeding could at least in part be due to the enhanced compression caused by radiation cooling.
We discuss here the 5-phase Lee Model code for the focus operated in various gases generally and using examples drawn from D, D-T, He, Ne, N, O, Ar, Kr and Xe. For D, D-T and He a fully ionized model is used. For the heavier gases from Ne onwards a corona model is used to generate the thermodynamic data required in the computation.

2. Introduction to the Lee model code

The Lee model code couples the electrical circuit with plasma focus dynamics, thermodynamics, and radiation, enabling a realistic simulation of all gross focus properties. The basic model, described in 1984 [9], was successfully used to assist several projects [10-13]. Radiation-coupled dynamics was included in the five-phase code, leading to numerical experiments on radiation cooling [15]. The vital role of a finite small disturbance speed discussed by Potter in a *Z*-pinch situation [15] was incorporated together with real gas thermodynamics and radiation-yield terms. This version of the code assisted other research projects [16-21] and was web published in 2000 [22] and 2005 [23]. Plasma self-absorption was included in 2007 [22], improving the SXR yield simulation. The code has been used extensively in several machines including UNU/ICTP PFF [3,12-14,16,18-21], NX2 [3,6,17,24], and NX1 [3,6,25] and has been adapted for the Filippov-type plasma focus DENA [26]. A recent development is the inclusion of the neutron yield Y_n using a beam–target mechanism [27-31], incorporated in recent versions [8,32] of the code (versions later than RADPFV5.13), resulting in realistic Y_n scaling with I_{pinch} [33-37]. The versatility and utility of the model are demonstrated in its clear distinction of I_{pinch} from I_{peak} [29] and the recent uncovering of a plasma focus pinch current limitation effect [30,31], as static inductance is reduced towards zero. Extensive numerical experiments had been carried out systematically resulting in the uncovering of neutron [27,28,36] and SXR [38-44] scaling laws over a wider range of energies and currents than attempted before. The numerical experiments also gave insight into the nature and cause of ‘neutron saturation [28,34,36,44]. The description, theory, code, and a broad range of results of this “Universal Plasma Focus Laboratory Facility” are available for download from [8,32].

A brief description of the 5-phase model is given in the following.

2.1 The 5-phases

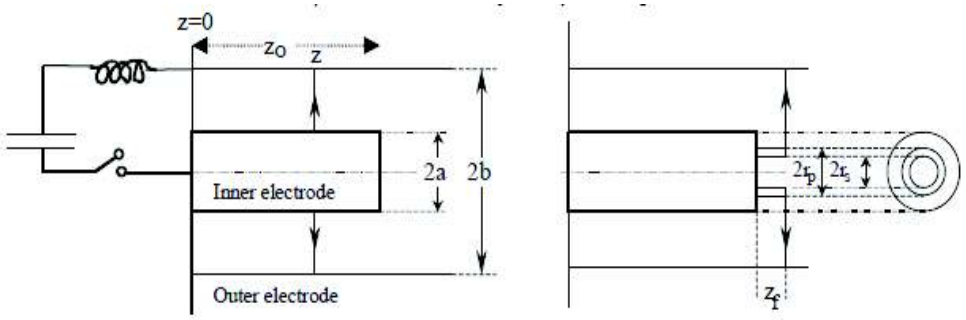

Figure 1. Schematic of the axial and radial phases. The left section depicts the axial phase, the right section the radial phase. In the left section, z is the effective position of the current sheath-shock front structure. In the right section r_s is the position of the inward moving shock front driven by the piston at position r_p. Between r_s and r_p is the radially imploding slug, elongating with a length z_f. The capacitor, static inductance and switch powering the plasma focus is shown for the axial phase schematic only.

The five phases (*a-e*) are summarised [8,29,32-36,38, 42-44] as follows:
a. Axial Phase (see Figure 1 left part): Described by a snowplow model with an equation of motion which is coupled to a circuit equation. The equation of motion incorporates the axial phase model parameters: mass and current factors f_m and f_c. The mass swept-up factor [45,46] f_m accounts for not only the porosity of the current sheet but also for the inclination of the moving current sheet-shock front structure, boundary layer effects, and all other unspecified effects which have effects equivalent to increasing or reducing the amount of mass in the moving structure, during the axial phase. The current factor f_c accounts for the fraction of current effectively flowing in the moving structure (due to all effects such as current shedding at or near the back-wall, and current sheet inclination).
b. Radial Inward Shock Phase (see Figure 3 right part): Described by 4 coupled equations using an elongating slug model. The first equation computes the radial inward shock speed from the driving magnetic pressure. The second computes the axial column elongation speed. The third computes the speed of the current sheath (magnetic piston), allowing the sheath to separate from the shock front by applying an adiabatic approximation [15]. The fourth is the circuit equation. Thermodynamic effects due to ionization and excitation are incorporated into these equations, these effects being particularly important for gases other than hydrogen and deuterium. Temperature and number densities are computed using shock-jump equations. A communication delay between shock front and current sheath due to the finite small disturbance speed [8,15] is implemented. The model parameters, radial phase mass swept-up and current factors f_{mr} and f_{cr} are incorporated in all three radial phases.
c. Radial Reflected Shock (RS) Phase: When the shock front hits the axis, because the plasma is collisional, a reflected shock develops which moves radially outwards, whilst the radial current sheath continues to move inwards. Four coupled equations are also used, these being for the reflected shock moving radially outwards, the piston moving radially inwards, the elongation of the annular column and the circuit. The plasma temperature behind the reflected shock undergoes a jump by a factor of 2. Number densities are computed using reflected shock jump equations.
d. Slow Compression (Quiescent) or Pinch Phase: When the out-going reflected shock hits the inward moving piston, the compression enters a radiative phase. For gases such as neon, radiation emission may enhance the compression as energy loss/gain terms from Joule heating

and radiation are included in the piston equation of motion. Three coupled equations are used; these being for piston radial motion, pinch column elongation and for the circuit. The duration of this slow compression phase is set as the time of transit of small disturbances across the pinched plasma column. The computation of this phase is terminated at the end of this duration.

e. Expanded Column Axial Phase: To simulate the current trace beyond this point we allow the column to suddenly attain the radius of the anode, and use the expanded column inductance for further integration. In this final phase the snow plow model is used, and two coupled equations are used similar to the axial phase above. This phase is not considered important as it occurs after the focus pinch.

We note [38,42,43] that in radial phases *b, c* and *d*, axial acceleration and ejection of mass caused by necking curvatures of the pinching current sheath result in time-dependent strongly center-peaked density distributions. Moreover the transition from phase *d* to phase *e* is observed in laboratory measurements to occur in an extremely short time with plasma/current disruptions resulting in localized regions of high densities and temperatures [47]. These centre-peaking density effects and localized regions are not modeled in the code, which consequently computes only an average uniform density and an average uniform temperature which are considerably lower than measured peak density and temperature. However, because the four model parameters are obtained by fitting the computed total current waveform to the measured total current waveform, the model incorporates the energy and mass balances equivalent, at least in the gross sense, to all the processes which are not even specifically modeled. Hence the computed gross features such as speeds and trajectories and integrated soft x-ray yields have been extensively tested in numerical experiments for several machines and are found to be comparable with measured values.

3 Plasma Focus Operation in xenon for production of EUV for NGL Next Generation Lithography

We wish to use the Lee Model code to run the 3 kJ UNU ICTP PFF (using its capacitor bank but with modification to the electrodes as required) in xenon to determine the conditions for good EUV yield, noting that the required standard NGL (next generation lithography) wavelength has been set at 13.5nm. A search through the NIST database [48] shows that the Xe ions suitable for the production of strong lines around 13.5nm are XeIX, XeX and XeXI; particularly XeXI. To determine the suitable temperature for XeXI we first ran a corona [49] calculation and obtained the following ionization curves in Figure.2.

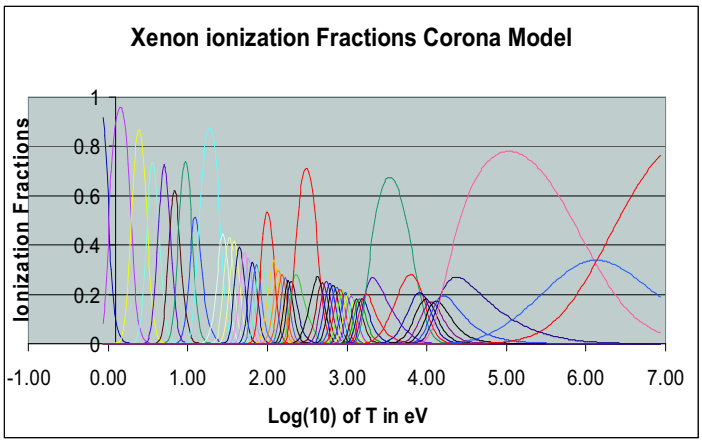

Fig 2 Ionization curves of xenon using a corona model

From Fig 2 we estimate that the temperature required to reach XeXI is around 30eV or less than 0.4×10^6K. Xe being a heavy gas with atomic mass of 84 requires very low shock speeds to reach this temperature. We also use the data of Fig 2 and the ionization energies and computed excitation energies to obtain the curves for the specific heat ratio γ [50] and the effective charge number Z_{eff} as functions of the temperature; as these thermodynamic data is needed for the code.
We used the electrical parameters of the UNU ICTP PFF (15kV. 114nH 12 mΩ), ran a series of numerical experiments varying tube parameters and found optimum conditions for reaching pinch temperatures of around 30 eV with axial speed of around 1.3 cm/us. Because of the low axial speed we had to alter the anode geometry to a=1.5cm. z_0=3 cm and also reduce voltage to V_0=10-12 kV. Under these conditions the effective charge number in the pinch is Z_{eff}~10 so that the pinch had the optimum species XeXI for 13.5nm. Under these conditions intense line radiation was computed around 40 J at 2 kJ storage energy (2% efficiency) and there was evidence from the computation that the line emission was affecting the dynamics, in other words the computed trajectory showed signs of radiation cooling leading to radiative collapse.
However for this purpose of generating EUV at 13.5 nm, such low speeds are required that it became obvious that the plasma focus may not have an advantage in this situation. The main lesson learned in these series of numerical experiments is that the model appeared capable of computing the gross dynamics of a radiation cooled pinch. This capability may become more important for the next example highlighted in this paper.

4 Thermodynamic Processes in krypton-doped deuterium for neutron enhancement

Recently Rishi Verma et al (2008) showed that a deuterium plasma doped with small amounts of krypton showed an order-of-magnitude enhancement in neutron emission. An attempt was made [51] to explain the enhancement through thermodynamic effects.

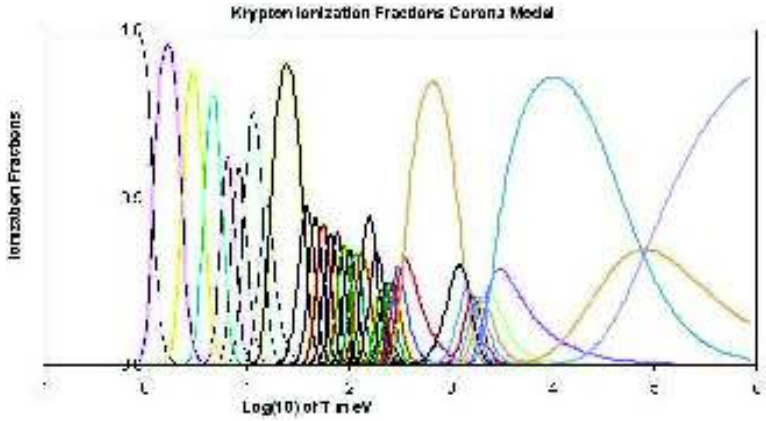

Figure 3 Ionization Curves for Krypton

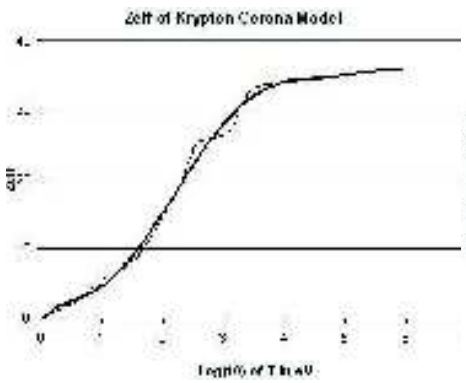

Figure 4a Z_{eff} of Kr

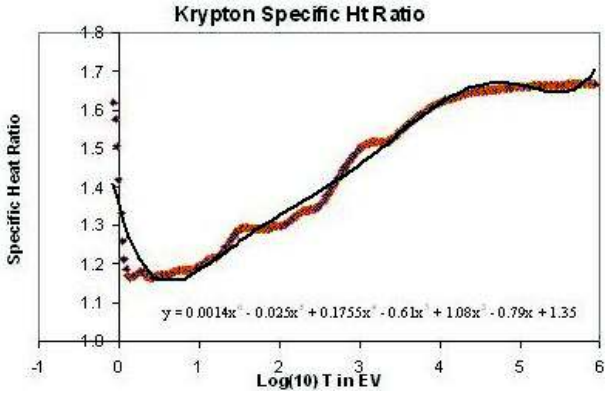

Figure 4b Specific Heat Ratio γ of Kr

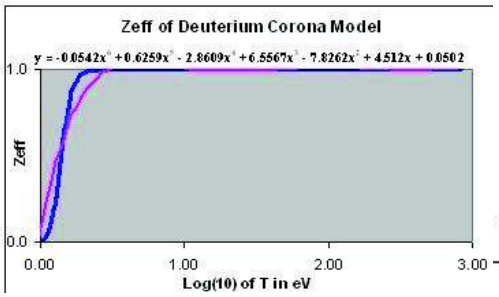

Figure 5a Z_{eff} of D

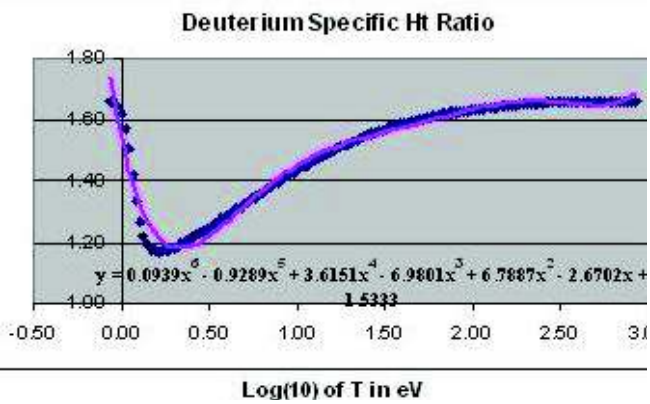

Figure 5b Specific Heat Ratio γ of D

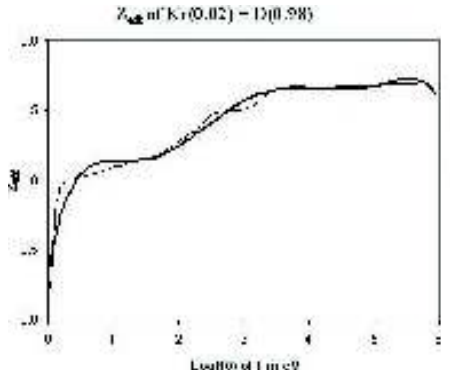

Figure 6a Z_{eff} of Kr-doped D

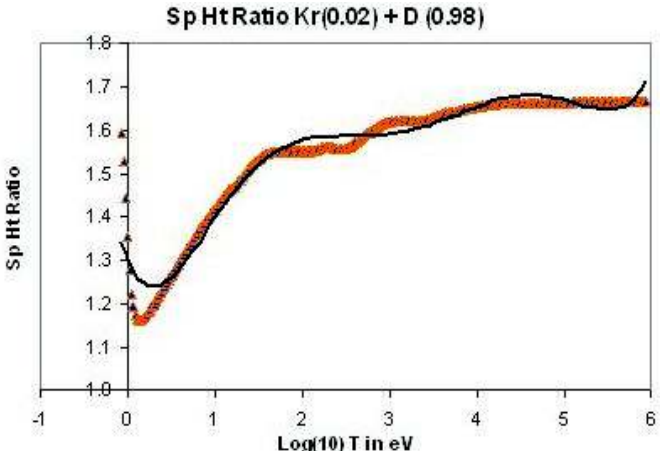

Figure 6b Specific Heat Ratio γ of Kr-doped D

Figure 3 shows the ionization curves of Kr computed from the corona model. Figure 4a shows the Z_{eff} of Kr obtained from Figure 3 whilst Figure 4b shows the computed specific heat ratio γ [50] of Kr computed from Figure 3 and the ionization and excitation energies of Kr. Figure 5a shows the Z_{eff} of D obtained from the ionization curves of D (not shown) whilst Figure 5b shows the specific heat ratio of D. Figure 6a shows the computed values of Z_{eff} for 2% Kr-doped D whilst Figure 6b shows the specific heat ratio of 2% Kr-doped D. The computed value of specific heat ratio for Kr-doped D is much reduced compared with that of pure D. For example at 20 eV ~$0.2x10^6$K the specific heat ratio of the mixture is less than 1.5 whereas that of pure D is already close to 1.6. This would enhance the shock compressed density to 5 for the 2% Kr-doped D,

instead of 4 for pure D. Clearly the increased compression would cause an enhancement to neutron yield.
The thermodynamic data of the Kr-doped D was fed into the Lee Model code. Indeed neutron yield enhancement was observed in the computed results. However the enhancement was less than a factor of 2 [51]; whereas the measured enhancement was by a factor of more than 10.
Thus the enhancement of neutron yield through increased compression due to thermodynamic effect was insufficient to explain the observed yield enhancement.
We proceeded to look at the possibility of radiation cooling and collapse in Kr as a possible mechanism for the further enhancement of neutron yield in a Kr-doped D.

5 Radiation Cooling and Collapse in krypton

The Pease-Braginskii current [52,53] is the value of current (1.6 MA) at which the Bremsstrahlung radiation (considered as a loss from the plasma) equals the Joule heating of the plasma pinch column in hydrogen assuming Spitzer resistivity [54]. When pinch current exceeds this value, the Bremsstrahlung losses exceed Joule heating and the plasma pinch begins to experience radiative cooling effects at progressively higher currents, until in severe cases, radiative collapse may be observed.. The P-B current only considers Bremsstrahlung, since at the high temperatures experienced in the hydrogen or deuterium pinch, the gases are fully ionized and there is no line radiation.
For gases such as neon, argon, krypton and xenon, there may still be line radiation even at the high pinch temperatures. This line radiation may considerably exceed the effect of Bremsstrahlung in terms of radiation cooling. In that case, the effect of radiation cooling, and eventually radiative collapse may be exacerbated; and may occur at much lower currents [55,56]. In other words the 'Pease-Braginskii' or threshold current, for these heavier gases may be much lower than the threshold (or P-B) current applied to hydrogen.

5a Power Densities:

We consider the following power respectively Joule heating, Bremsstrahlung and Line radiation generated in a plasma column of radius r_p, length l at temperature T:

$$\frac{dQ_J}{dt} = C_J T^{-3/2} \frac{l}{\pi r_p^2} Z_{eff} I^2 \quad \text{where } C_J \cong 1300 \text{ and } T \text{ is in Kelvin} \tag{1}$$

$$\frac{dQ_{Brem}}{dt} = C_1 T^{1/2} n_i^2 Z_{eff}^3 \pi r_p^2 l \quad \text{where } n_i \text{ is in m}^{-3} \text{ and } C_1 = 1.6 \times 10^{-40} \tag{2}$$

$$\frac{dQ_{line}}{dt} = C_2 T^{-1} n_i^2 Z_n^4 Z_{eff} \pi r_p^2 l \quad \text{where } C_2 = 4.6 \times 10^{-31} \tag{3}$$

To see the relative magnitudes of these power terms as a function of T we plot the magnitudes of these terms in Fig 7. We note from Fig 7 that in the range of plasma focus operation (typically left of 1 keV) recombination radiation power is much less than line radiation power. Hence in the following analysis we will not consider recombination power. For the radiation power terms [57] we take Bremsstrahlung as the reference so that we compare line radiation power with Bremstrahlung power and from that comparison we are able to deduce a simple comparative expression as follows.

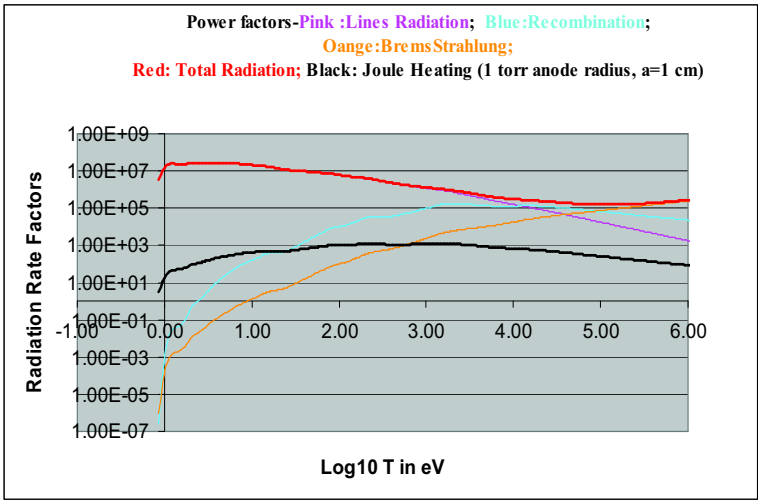

Figure 7 Showing the relative importance of power gain/loss terms as a function of temperature. Plasma Focus operation is at temperatures lower than 10^7K or left of log (10) T = 3.00 in the above graph. The example here is computed for xenon for 1 Torr with an anode radius 'a' of 1cm.

We use the Bennett distribution to obtain a relationship between T and I as follows:

$$T = b\frac{I^2}{(n_i r_p^2)(1+Z_{eff})} \qquad \text{where} \quad b = \frac{\mu}{8\pi^2 k} \tag{4}$$

Hence we re-write the power terms as follows:

$$\frac{dQ_J}{dt} = \frac{C_J(1+Z_{eff})^{3/2}}{b^{3/2}} \frac{n_i^{3/2}}{I} r_p \frac{l}{\pi} Z_{eff} \tag{5}$$

$$\frac{dQ_{Brem}}{dt} = -\pi C_1 b^{1/2} n_i^{3/2} \frac{Z_{eff}^3}{(1+Z_{eff})^{1/2}} r_p l \; I \tag{6}$$

$$\frac{dQ_{line}}{dt} = \frac{-\pi C_2}{b} n_i^3 r_p^4 (1+Z_{eff}) Z_{eff} \frac{Z_n^4 l}{I^2} \tag{7}$$

Total Power is written adding these 3 terms:

$$\frac{dQ}{dt} = -\pi\left[C_1 b^{1/2}\right] \frac{Z_{eff}^3}{(1+Z_{eff})^{1/2}} n_i^{3/2} r_p l \; I - \frac{\pi C_2}{b}(1+Z_{eff}) Z_{eff} Z_n^4 n_i^3 r_p^4 \frac{l}{I^2} + \frac{C_J}{\pi b^{3/2}}(1+Z_{eff})^{3/2} Z_{eff} n_i^{3/2} r_p \frac{l}{I} \tag{8}$$

5b Check for value of Pease-Braginskii current $I_{P\text{-}B}$

From (8) if we consider only the two terms, Joule heating power and the Bremsstrahlung power; then putting that version of equation (8) to zero we obtain the threshold current as:

$$I_{p-B}^2 = \frac{C_J}{C_1\pi^2 b^2}\frac{(1+Z_{eff})^2}{Z_{eff}^2} = \frac{4C_J}{C_1\pi^2 b^2} \tag{9}$$

Noting that for hydrogen Z_{eff}=1; and $I_{P\text{-}B}$ computes correctly to a value of 1.6 MA.

5c Line Radiation greatly reduces the threshold current

Considering the general case with all three power terms of equation (8) we obtain:

$$I^2 = \frac{C_J(1+Z_{eff})^2}{C_1\pi^2 b^2 Z_{eff}^2} \times \frac{C_1 Z_{eff}^2}{\left[C_2 z_n^4 T^{-3/2} + C_1 Z_{eff}^2\right]} \tag{10}$$

So that we may write:

$$I^2 = \frac{I_{p-B}^2}{4} \times \frac{1}{\left[\frac{C_2 z_n^4 T^{-3/2}}{C_1 Z_{eff}^2} + 1\right]} \times \frac{(1+Z_{eff})^2}{Z_{eff}^2} \tag{11}$$

Noting that

$$\frac{C_2 z_n^4 T^{-3/2}}{C_1 Z_{eff}^2} = \frac{dQ_{line}/dt}{dQ_{Brem}/dt} \tag{12}$$

We may also write

$$I^2 = I_{p-B}^2 \times \frac{1}{K} \tag{13}$$

Where

$$K = 4\left[\frac{(dQ_{line}/dt) + (dQ_{Brem}/dt)}{(dQ_{Brem}/dt)}\right] \tag{14}$$

where the factor $Z_{eff}^2 / (1+ Z_{eff})^2$ ~1 since Z_{eff} has the value >10 for typical plasma focus operation in Ar, Kr and Xe; even in Ne, Z_{eff} is close to 10.

We note from Figure 7 that in plasma focus operation in a heavy noble gas, typically say in the range 100 to 1000 eV the ratio of line power to Bremsstrahlung power has the range 1000 times to 10 times; so the threshold current is reduced from $I_{P\text{-}B}$ by a factor of ~30 at 100eV to ~3 times at 1000 eV; ie to ~50 kA at 100eV to ~500 kA at 1000 eV. In other words at the lower temperature end of plasma focus operation in a gas like Kr or Xe a current of 50kA may be enough to reach the threshold at which line radiation begins to exceed joule heating. This greatly reduced threshold current is reflected in Equ 13 where the reduction factor K is seen in (14) to be a large factor since line radiation greatly exceeds Bremsstrahlung.

5d Effect of plasma self-absorption

We also note that the above consideration has not taken into account the effect of plasma self-absorption. Taking that into consideration the emission power will be reduced, effectively reducing the value of K. In other words, plasma self absorption will raise the threshold current from that value computed in Equ (13). We have included radiation-coupled dynamics as well as plasma self-absorption into the Lee Model code (8). This is described in the following sections.

6 Lee Model code with radiation-coupled dynamics and plasma self-absorption

6a Radiation-coupled dynamics

The Lee Model code incorporates radiation-coupled dynamics (8) using the following equation:

$$\frac{dr_p}{dt} = \frac{\frac{-r_p}{\gamma I}\frac{dI}{dt} - \frac{1}{\gamma+1}\frac{r_p}{Z_f}\frac{dZ_f}{dt} + \frac{4\pi(\gamma-1)}{\mu\gamma Z_f}\frac{r_p}{f_c^2 I^2}\frac{dQ}{dt}}{\frac{\gamma-1}{\gamma}} \tag{15}$$

where dQ/dt is computed from Equation (8)

6b Plasma self-absorption

Plasma self-absorption [8,58-62] is included by computing the value of plasma self-absorption correction factor A_{ab} where

$$A_{ab} = \left[(1 + 10^{-20} n_i Z_{eff})\right]^{-(1+M)} \tag{16}$$

where T_{ev} is the temperature in eV and M is the photonic excitation number:

$$M = 1.66 \times 10^{-16} r_p Z_n^{1/2} n_i / (Z_{eff} T_{eV}^{1.5}) \tag{17}$$

When there is no plasma self-absorption A_{ab} =1. When A_{ab} goes below 1, plasma self absorption starts. When a sizeable fraction of the photons is re-absorped e.g. value of A_{ab} reaches 1/e, plasma radiation is considered to switch over from volume radiation to surface radiation and is computed accordingly in the model.
Thus the code is able to within its modelling compute the amount of radiation emitted, inclusive of plasma self absorption effects, incorporating these effects into the plasma dynamics.

7 Numerical Experiment in krypton demonstrating radiative collapse

We carried out numerical experiments using the Lee Model code which includes the effect of plasma self absorption; for the UNU ICTP PFF (30 μF, 110 nH, 12 mΩ resistance, b=3.2 cm, a=0.95 cm, z_0=16 cm) operated at 12 kV neon at varying pressures from 0.1 -2.0 Torr; so as to demonstrate radiative cooling leading to radiative collapse. Radial trajectories are shown in Figure 8 a-f.

It is clear from Figure 8 that radiative cooling reduces the pinch radius as pressure is increased, above 0.1 torr. Strong radiative collapse is evident in the range 0.5 to 1.6 torr (Figs 8b-8e).

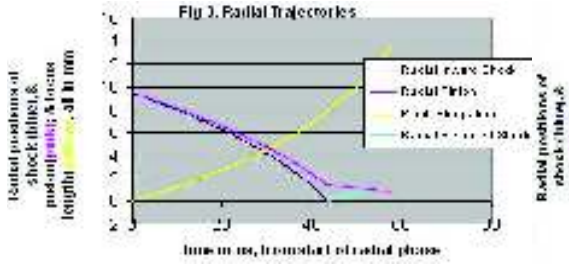

Figure 8a 0.1 Torr

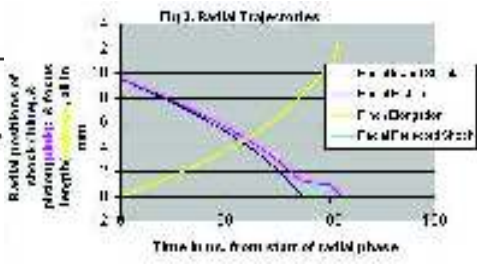

Figure 8b 0.5 Torr

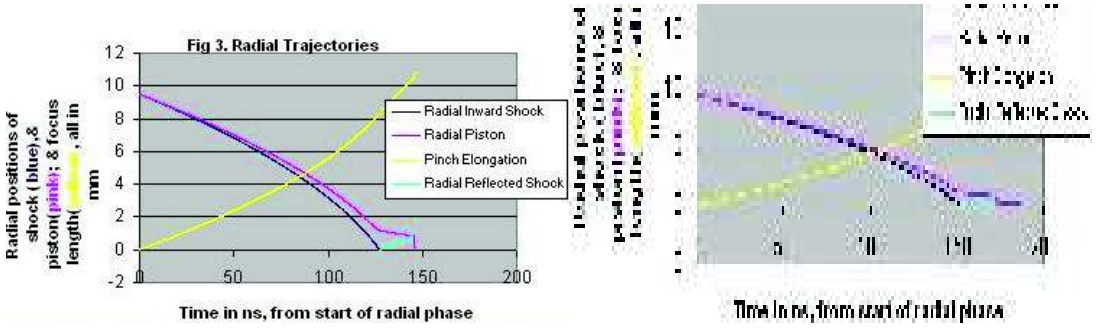

Figure 8c 0.9 torr

Figure 8d 1.1 torr

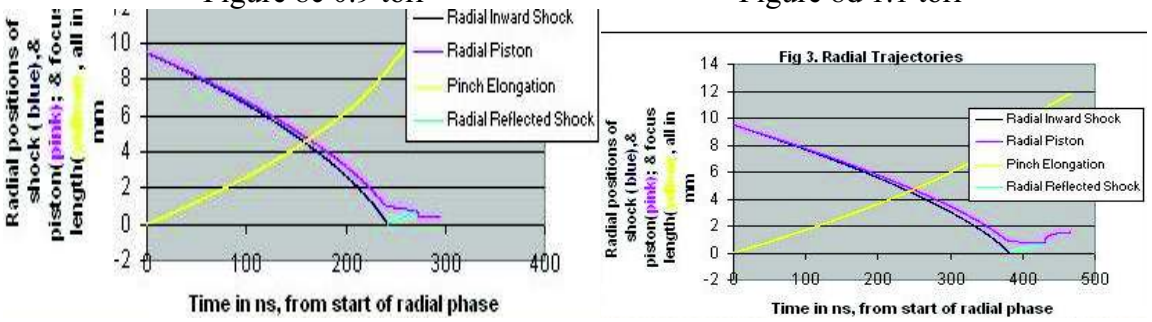

Figure 8e 1.6 torr

Figure 8f 2 torr

Figure 8a acts as a reference situation and shows the radial dynamics at 0.1 torr. The radial inward shock wave starts at 9.5 mm and is driven to the axis after 43 ns with the driving magnetic piston trailing it by some 1.5 mm as the shock front hits reaches the axis. A reflected shock RS goes outwards and after some 9 ns hits the incoming piston. At this time the pinch starts and the column compresses inwards a little, as is typical Computed data indicates that even in this shot the radiation power emitted (mostly line) already exceeds the Joule heating power with the pinch temperature in this shot reaching 1.5 keV. This means that there is already net power loss (or radiation cooling) but the radiation cooling insufficient to perceptibly affect the dynamics at the pinching power provided by the available pinch current at that time. At 0.5 torr and a pinch temperature of 520 eV with a pinch current of just under 100 kA, radiative collapse is obvious with the radius collapsing in a few ns to the cut-off radius of 0.1mm set in the model. At 0.9 torr with a pinch temperature of 300 eV and a pinching current of just 80 kA, the radiative collapse is so strong as to produce collapse to cut-off radius within less than 1 ns. At 1.1 torr with a pinch temperature of 220 eV, the collapse does not reach the cut-off radius. In this case the

model maintains a small radius (0.2 mm) pinch for about 10ns. These are the conditions (high density, relatively long pinch duration) which produce huge line yields of more than 100J. At 1.6 torr and pinch temperature of 105 eV with a pinch current of just 60 kA, the speeds are much slower now and the pinch occurs late so the current has dropped considerably reducing the pinching force; the radiative collapsed radius is now bigger (0.6 mm). Finally at 2 torr, the column blows out instead of pinching in as the RS hits the piston.

8 Conclusions:

This paper considers new modelling situations including the following: (1). Plasma Focus operation in Xe for production of EUV. The low speeds required for optimum yield suggest that the PF has no advantage for this purpose. (2). Neutron yield enhancement in Kr-doped D as a result of thermodynamic effects of increased Z_{eff} and reduced Sp Ht Ratio. The computations [51] suggest that the yield enhancement from the reduced Sp Ht Ratio is less than a factor of 2 and cannot explain the factor of greater than 10 times yield enhancement that has been measured in a 2% Kr-doped D. (3). Radiative cooling leads to radiative collapse of the Kr pinch. The Lee Model code includes the effect of energy gain/loss into its dynamics, moreover incorporates the effect of plasma self-absorption. The code was run in Kr and demonstrates radiative cooling leading to radiative collapse at a pinch current ranging from 60-100 kA. It is suggested that similar radiative collapse effects could be operative in Kr-doped D, more probably in localized regions rather than over the whole pinch. Such a mechanism may explain the observed yield enhancement.

References

1. Bernard A., Bruzzone H., Choi P., Chuaqui H., Gribkov V., Herrera J., Hirano K., Krejci A., Lee S., Luo C., Mezzetti F., Sadowski M., Schmidt, H., Ware, K., Wong, C.S., Zoita, V. (1998) Scientific Status of Plasma focus Research. *Moscow J Physical Society,* **8***,* 93-170.
2. Rahul R. Prasad, Mahadevan Krishnan et al, Neon Dense Plasma Focus Point X-ray source for < 0.25μm Lithography*, SPIE* **2194**, 120-128 (1994)
3. Lee S., P. Lee, Zhang G., Feng X., Gribkov V. A., Liu M., Serban A., and Wong T., High rep rate high performance plasma focus as a powerful radiation source, *IEEE Trans. Plasma Sci.*, 1998, ***26***, no. 4, pp. 1119–1126.
4. Bergmann, K., Rosier O., Neff W. and Lebert, R. (2000) Pinch-Plasma Radiation Source for Extreme-Ultraviolet Lithography with a Kilohertz Repetition Frequency. *Applied Optics*, **39**, Issue 22, pp. 3833-3837.
5. R. Lebert[1], W. Neff[2], D. Rothweiler. (1996) Pinch Plasma Source for X-Ray Microscopy with Nanosecond Exposure Time Journal of X-Ray Science and Technology Volume 6, Number 2.
6. Gribkov, V.A., Srivastava, A., Keat, P.L.C. Kudryashov, V. Sing Lee. (2002) Operation of NX2 dense plasma focus device with argon filling as a possible radiation source for micro-machining Plasma Science, IEEE Transactions on **30**, 1331 – 1338.
7. K N Koshelev, V I Krauz, N G Reshetniak, R G Salukvadze, Yu V Sidelnikov, E Yu Khautiev. (1988). The formation of the micropinch structure in plasma focus by the addition of heavy impurities *J. Phys. D: Appl. Phys.* **21** 1827.
8. Lee S. (2010) Radiative Dense Plasma Focus Computation Package: RADPF. http://www.plasmafocus.net http://www.plasmafocus.net/IPFS/modelpackage/File1RADPF.htm

9. Lee, S. (1984) Plasma focus model yielding trajectory and structure. In *Radiations in Plasmas*, McNamara, B., Ed.; World Scientific, Singapore: Volume **II**, pp. 978–987.
10. Tou, T. Y.; Lee, S.; Kwek, K. H. (1989) Non perturbing plasma focus measurements in the run-down phase. *IEEE Trans. Plasma Sci.* **17**, no. 2, 311–315.
11. Lee, S. (1991) A sequential plasma focus. *IEEE Trans. Plasma Sci.*, ***19***, no.5,
12. Lee, S.; Tou, T. Y.; Moo, S. P.; Eissa, M. A.; Gholap, A. V.; Kwek, K. H.; Mulyodrono, S.; Smith, A. J.; Suryadi, S.; Usada, W.;. Zakaullah, M. (1988) A simple facility for the teaching of plasma dynamics and plasma nuclear fusion. *Amer. J. Phys.* ***56,*** no. 1, 62–68.
13 Lee S. and Serban A. (1996). Dimensions and lifetime of the plasma focus pinch. *IEEE Trans. Plasma Sci.*, ***24***, no. 3, 1101–1105.
14. Jalil bin Ali. (1990) *Development and studies of a small plasma focus*, Ph.D. Dissertation; Universiti Teknologi Malaysia, Malaysia,
15 Potter, D. E. (1978). The formation of high-density z-pinches. *Nucl. Fusion.* ***18***, 813–823.
16. Liu M., (2006) "Soft X-rays from compact plasma focus," Ph.D. dissertation, NIE, Nanyang Technological Univ., Singapore, ICTP Open Access Archive. [Online]. Available: http://eprints.ictp.it/327/
17. Bing S. (2000) "Plasma dynamics and X-ray emission of the plasma focus," Ph.D. dissertation, NIE, Nanyang Technological Univ., Singapore, 2000. ICTP Open Access Archive. [Online].: http://eprints.ictp.it/99/.
18. Serban A. and Lee S. (1998) "Experiments on speed-enhanced neutron yield from a small plasma focus," *J. Plasma Phys.*, ***60***, no. 1, pt. 1, pp. 3–15.
19. Liu M.H., Feng X.P., S. V. Springham, and Lee S. (1998) "Soft X-ray measurement in a small plasma focus operated in neon," *IEEE Trans. Plasma Sci.*, ***26***, no. 2, pp. 135–140.
20. Lee S. (1998) in *Twelve Years of UNU/ICTP PFF—A Review*. Trieste, Italy: Abdus Salam ICTP, pp. 5–34. IC/ 98/ 231, ICTP Open Access Archive. [Online]. Available: http://eprints.ictp.it/31/
21. Springham S. V., Lee S., and Rafique M. S.(2000) "Correlated deuteron energy spectra and neutron yield for a 3 kJ plasma focus," *Plasma Phys. Control. Fusion*, **42***,* no. 10, pp. 1023–1032.
22. Lee S. (2010). [Online]. Available: http://ckplee.myplace.nie.edu.sg/plasmaphysics/
23. Lee S. (2005) *ICTP Open Access Archive*, [Online]. Available: http://eprints.ictp.it/85/
24. Wong D., Lee P., Zhang T., Patran A., Tan T. L., Rawat R. S., and Lee S. (2007) "An improved radiative plasma focus model calibrated for neonfilled NX2 using a tapered anode," *Plasma Sources Sci. Technol.* ***16***, no. 1, pp. 116–123
25. Bogolyubov E. P., Bochkov V. D., Veretennikov V. A., Vekhoreva L. T., Gribkov V. A., Dubrovskii A. V., Ivanov Y. P., Isakov A. I, Krokhin O. N., Lee P., Lee S., Nikulin V. Y., Serban A., Silin P. V., Feng X., and Zhang G. X. (1998) "A powerful soft X-ray source for X-ray lithography based on plasma focusing," *Phys. Scr.*, ***57***, no. 4, pp. 488–494.
26. Siahpoush V., Tafreshi M. A., Sobhanian S., and Khorram S. (2005) "Adaptation of Sing Lee's model to the Filippov type plasma focus geometry," *Plasma Phys. Control. Fusion*, ***47***, no. 7, pp. 1065–1075.
27. Lee S. and Saw S. H. (2008) "Neutron scaling laws from numerical experiments," *J. Fusion Energy*, ***27***, no. 4, pp. 292–295.
28. Lee S., (2008) "Current and neutron scaling for megajoule plasma focus machines," *Plasma Phys. Control. Fusion*, ***50***, no. 10, p. 105 005 (14pp).
29. Lee S., Saw S. H., Lee P. C. K., Rawat R.S., and Schmidt H., (2008) "Computing plasma focus pinch current from total current measurement," *Appl. Phys. Lett.*, ***92***, no. 11, p. 111 501.
30. Lee S. and Saw S. H., (2008) "Pinch current limitation effect in plasma focus," *Appl. Phys. Lett.*, ***92***, no. 2, p. 021 503.

31. Lee S., Lee P., Saw S. H., and Rawat R. S., (2008) "Numerical experiments on plasma focus pinch current limitation," Plasma Phys. Control. Fusion **50** 065012 (8pp)
32. Web-site: http://www.intimal.edu.my/school/fas/UFLF/ 2010
33. Saw S. H. and Lee S. (2009) "Scaling laws for plasma focus machines from numerical experiments". Invited paper: IWPDA, Singapore.
34. Lee S. (2009) Diagnostics and Insights from Current waveform and Modelling of Plasma Focus. Keynote address: IWPDA, Singapore.
35. Saw S. H. and Lee S. (2009) "Scaling the plasma focus for fusion energy considerations". Tubav Conferences: Nuclear & Renewable Energy Sources, Ankara, Turkey.
36. Lee S. (2009) "Neutron Yield Saturation in Plasma Focus-A fundamental cause" *Appl. Phys. Lett*., 2009, ***95***, 151503 published online.
37. Lee S., Saw S. H., Soto L., Moo S. P., Springham S. V.(2009) Numerical experiments on plasma focus neutron yield versus pressure compared with laboratory experiments, *Plasma Phys. Control. Fusion***, *51*** 075006 (11pp).
38. Lee S., Saw S. H., Lee P. & Rawat R. S. (2009) "Numerical Experiments on Neon plasma focus soft x-rays scaling", *Plasma Physics and Controlled Fusion*, ***51***, 105013 (8pp).
39. Akel M., Al-Hawat Sh., Lee S. (2010) "Pinch Current and Soft x-ray yield limitation by numerical experiments on Nitrogen Plasma Focus". *J Fusion Energy*, **29**, 94
40, Akel M., Al-Hawat Sh., Lee S. (2009) "Numerical Experiments on Soft X-ray Emission Optimization of Nitrogen Plasma in 3 kJ Plasma Focus SY-1 Using Modified Lee Model", *J Fusion Energy* DOI 10.1007/s10894-009-9203-4 First online, May 19, 2009.
41. M. Akel, Sh. Al-Hawat, S. H. Saw and S. Lee. (2010) Numerical Experiments on Oxygen Soft X-Ray Emissions from Low Energy Plasma Focus Using Lee Model . J Fusion Energy , **29,** 223–231
42. Lee S., Rawat R. S., Lee P., S H Saw S. H., (2009) Soft x-ray yield from NX2 plasma focus, *J. Appl. Phys.*, ***106*****,** 023309.
43. Saw S. H., Lee P. C. K., Rawat R. S. & Lee S. (2009) 'Optimizing UNU/ICTP PFF Plasma Focus for Neon Soft X-ray Operation' *IEEE Trans on Plasma Sc*, ***37***, 1276-1282.
44. Sing Lee, Sor Heoh Saw, (2010) Numerical Experiments providing new Insights into Plasma Focus Fusion Devices, *Invited Review Paper: Special edition on "Fusion Energy" Energies* 2010, ***3***, 711-737.
45. Lee, S. (2004) *Characterising the Plasma Focus Pinch and Speed Enhancing the Neutron Yield.* In: First Cairo Conf Plasma Physics & Applications. International Cooperation Bilateral Seminars (Vol **34**). Forschungszentrum Juelich GmbH, Juelich, Germany, pp. 27-33. ISBN 3-89336-374-2; 912–919.
46. Chow S. P., Lee S., Tan B. C., Current sheath studies in a co-axial plasma focus gun .J. of Plasma Phys., 8: 21-31.
47. Favre M., Lee S., Moo S. P., Wong C. S. (1992) X-ray emission in a small plasma focus operating with H2-Ar mixtures, Plasma Sources Science and Technology, **1** 122-125.
48. http://physics.nist.gov/PhysRefData/Elements/
49. McWhirter (1965) in "Plasma Diagnostic Techniques" (Eds. Huddelstone, R H and Leonard S L). Academic Press, New York.
50. Lee, S (1983) Radius Ratios of Argon Pinches. Australian J Phys **35**, 391.
51. Tan, C. (2011) M.Sc thesis in progress
52. Pease, R. (1957) Procs Phys Soc. **70**, 11.
53. Braginskii, S. (1957) Zh Eksp Teor Fiz **33**, 645.
54. Spitzer, L. (1967) Physics of Fully ionized Gases. Interscience.
55. Koshelev, K. and Sidelnikov, Yu. (1985) A micropinch as a spectral source of highly ionized atoms. Nucl Instr Methods Phys Res B**9** 704-5

56. Koshelev, K. and Pereira, N. (1991) Plasma points and radiative collapse in vacuum sparks. J Appl. Phys. **69**, 21-44
57. Huddelstone, R H and Leonard S L (1965) in "Plasma Diagnostic Techniques" (Eds. Huddelstone, R H and Leonard S L). Academic Press, New York.
58 Robson, A E. (1991) Phys. Fluid B3, 1481
59 Bruzzone, H. (2001). Nucleonika **46**, S3
60 Bernal, L, Bruzzone H. (2002). Plasma Phys & Contr. Fusion, **41**, 223
61 Chittenden, (1995) Phys. Plasma, **2**, 1242.
62 Khattak, N A D. (2011) Anomalous Heating (LHDI). http://www.plasmafocus.net/IPFS/modelpackage/File3Appendix.pdf